RETAINING HIGH *Q* FACTORS IN ELECTRODE-LESS AlN-ON-Si BULK MODE RESONATORS WITH NON-CONTACT ELECTRICAL DRIVE

S M Enamul Hoque Yousuf[1†], Yuncong Liu[1†*], Xu-Qian Zheng[1], Afzaal Qamar[2], Mina Rais-Zadeh[2,3*], and Philip X.-L. Feng[1*]*

[1]Electrical & Computer Engineering, University of Florida, Gainesville, FL 32611, USA
[2]Electrical & Computer Engineering, University of Michigan, Ann Arbor, MI 48109, USA
[3]Jet Propulsion Laboratory, California Institute of Technology, Pasadena, CA 91109, USA

ABSTRACT

This paper reports on an experimental study of actuation techniques of aluminum nitride on silicon (AlN/Si) heterostructure resonant microelectromechanical systems (MEMS) with both bulk and flexural modes, and comparison of their quality factors (*Q*s) and energy losses induced by different resonant motion excitation schemes. For AlN/Si MEMS resonators without deposited top metal electrodes, we have devised a new scheme to electrically drive the device, enabled by a non-contact overhanging electrode inducing gradient forces, to replace the otherwise required optical excitation for electrode-less devices. For the bulk mode resonance of AlN/Si resonator at 10MHz, almost equal *Q* of ~26,000 is obtained for both the new electrical drive and the optical drive, whereas the electrical drive enables the detection of a ~1MHz mode that is not visible when driven optically. For the Si-only device, *Q* of 257,300 is attained with the non-contact electrical drive, noticeably higher than the *Q* of 212,225 with the optical drive, suggesting that non-contact electrical excitation results in lower energy dissipation than optical actuation. The present work motivates further studies of transduction mechanisms to achieve higher resonator *Q*s.

KEYWORDS

Actuation mechanism, aluminum nitride (AlN), micromechanical resonator, electrical drive, optical drive, piezoelectric resonator, quality factor (*Q*).

INTRODUCTION

Laterally vibrating AlN/Si bulk acoustic mode resonators (BARs) have emerged as enabling building blocks for future RF MEMS front-ends with application in communication, energy harvesting, and sensing [1,2]. In addition to combining excellent electromechanical coupling of AlN [3,4] and low acoustic loss of single-crystal Si, this structure is compatible with mainstream CMOS wafer-scale manufacturing [5,6] and exhibits high power handling capability. To fully benefit from excellent characteristics of AlN-on-Si MEMS resonators, it is advantageous to have a high *Q* to enable higher resolution sensing or higher performance frequency selection. However, it has been shown that the addition of AlN layer onto Si causes lowered *Q* in the AlN/Si devices as compared to the Si-only devices due to the columnar boundaries in the AlN piezoelectric layer [7]. The addition of metal electrodes on top of the AlN/Si heterostructure, as often needed for piezoelectric excitation and detection of resonant motions, can further degrade the *Q*. Therefore, achieving high *Q* in piezoelectrically driven AlN/Si resonators has been a major challenge. AlN/Si BARs without any top electrodes have been designed and investigated to reduce energy losses associated with loading and interfacial dissipation due to deposited metal electrodes atop. Although, without electrodes, such designs have not been conveniently driven by electrical signals, and thus far have been commonly excited by optical means.

In this study, we devise and demonstrate a non-contact external electrode, for efficient drive of the length extensional (LE) mode MEMS resonators fabricated in different heterostructure stacks. The excitation of device motion is attributed to the inverse piezoelectric effect and gradient forces exerted on polarized dipoles which emerge inside the material from the applied electrical field. The resonant behavior of heterostructure devices operating in both bulk or flexural modes have been experimentally examined by optical and electrical excitation schemes and their *Q*s and energy losses are also compared. The electrical drive used to actuate in-plane bulk mode of Si-only resonators results in a higher *Q* compared with that in the case of optical drive. The new technique of exciting the resonators without the need for electrical or mechanical contact enables convenient electrical drive and overcomes the limitations and losses associated with metal deposition. Further study and development of contact-less electrical actuation, as suggested herein, may help pave a way for attaining high-performance devices with improved *Q*s.

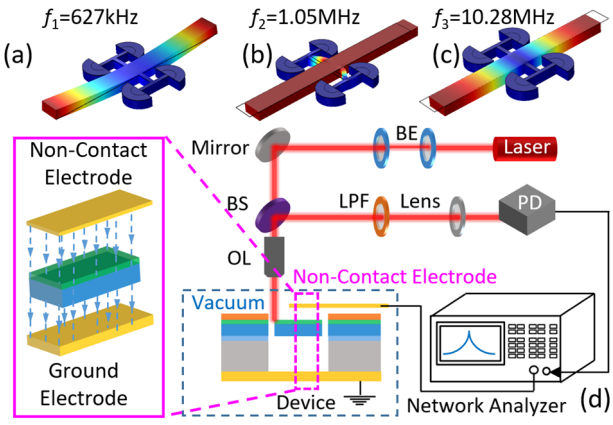

Figure 1: FEM simulated mode shapes of (a) the out-of-plane flexural mode, (b) the in-plane flexural mode, and (c) the LE bulk mode. (d) Schematic of non-contact electrical drive and optical 'knife-edge' detection (via a 633nm low-power laser) of the AlN/Si resonator. BS: beam splitter, BE: beam expander, PD: photodetector, LPF: long pass filter, OL: objective lens.

DEVICE DESIGN AND FABRICATION

Each device has a suspended structure supported by a pair of parallel tethers. Figure 1c illustrates the simulation

results of the fundamental in-plane bulk mode obtained using finite element modeling (FEM): two ends of the main body scale back and forth within the device plane, and the center of the main body in line with the tethers is the nodal plane. The resonance frequency of the LE mode resonator can be expressed as

$$f_0 = \frac{1}{2L}\sqrt{\frac{(t_1 E_{Y1} + t_2 E_{Y2})}{(t_1\rho_1 + t_2\rho_2)}}, \quad (1)$$

where t_1 (t_2), E_{Y1} (E_{Y2}), and ρ_1 (ρ_2) are the thickness, Young's modulus, and mass density of Si (AlN), respectively. The devices have length L and are designed to operate at f_0 = 10MHz in the LE mode.

As illustrated in Fig. 2, the fabrication of AlN/Si resonators starts with a double-side polished Si-on-insulator (SOI) wafer comprising a 20µm thick n-type phosphorus (P) doped (at 4.6 × 10^{19}cm^{-3}) Si device layer and a 500µm Si handle layer. 1µm thick AlN layer is then directly deposited on the highly doped Si layer to act as a piezoelectric layer. 100nm of aluminum (Al) is chosen for metal routing and patterned through lift-off process. We define the front-side patterns on the wafer using photolithography followed by reactive ion etching (RIE) through the buried oxide (BOX) layer. Suspended devices are realized via deep reactive ion etching (DRIE) from the wafer backside. Si-only devices are realized by removing the top deposited AlN piezoelectric layer as well as the metal electrodes.

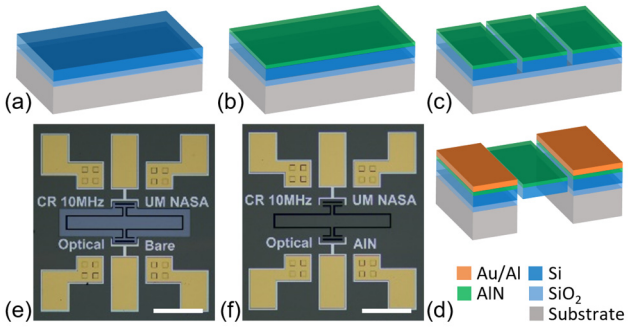

Figure 2: Illustrations of the AlN/Si device fabrication process: (a) SOI wafer. (b) Sputter deposition of AlN onto the SOI wafer. (c) Reactive ion etching (RIE) process to form the front-side pattern. (d) Al routing metal deposition followed by the removal of Si substrate and BOX layer to form free-standing structure. Optical images of (e) Si-only device and (f) AlN/Si device. Scale bar: 200µm.

ANALYSIS AND SIMULATIONS

Prior understanding of the theoretical framework of the new electrical drive scheme (Fig. 3a) is necessary to correctly interpret experimental results. Here, we perform COMSOL simulations to evaluate the electric field distribution. It is seen from Fig. 3b that the total electric field has leaned towards the tangential component as it goes across the air-AlN interface because of the difference in dielectric constants of the two mediums. Since AlN is a spontaneously polarized piezoelectric material, it possesses a net non-zero internal electric field when no external field is applied. Figure 3c shows a molecular sketch of AlN consisting of several dipoles arranged in z direction. When it is subjected to the applied electric field, the dipoles change length, generating a mechanical strain and thereby a change in dimensions of the material, due to the inverse piezoelectric effect. Thus, an RF electric field modulated by a network analyzer (NA) induces expansion and compression of the AlN, resulting in harmonic lateral vibrations. In crystalline Si layer, which is not commonly used as a dielectric material, the applied electric field shifts the negatively charged valence electrons with respect to the positive Si core. Therefore, electronic polarization arises in Si and a polarization vector develops along the applied field (Fig. 3d). Since there is a gradient in the electric field, the induced dipoles will experience forces in both z and x direction, often called gradient forces (Fig. 3e) [8]. The direction of this force varies with different field directions. Hence an alternating RF field gives rise to oscillating forces and consequently the actuation of both in-plane and out-of-plane motions.

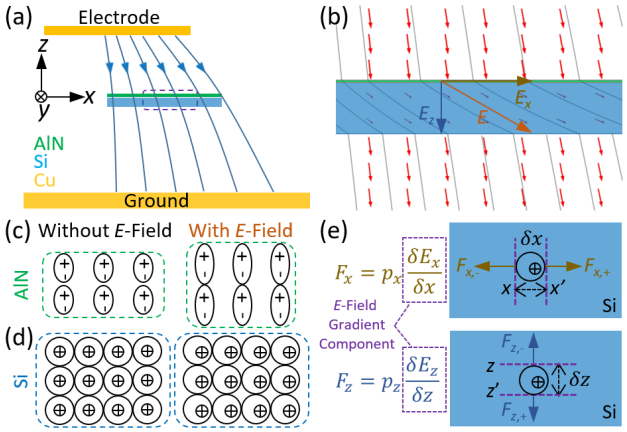

Figure 3: Mechanism of non-contact electrical drive. (a) Illustration of the AlN/Si resonator placed inside the electric filed. (b) Zoom-in view of the purple dashed box shown in (a) presents the field lines deviation from the lines outside the device. (c) Dipole arrangement in AlN and (d) atomic structure in Si before and after applying electric field, respectively. (e) Gradient forces responsible for in-plane and out-of-plane motions originate from the net forces acting on two opposite charges in Si layer.

To characterize the resonant behavior of the LE mode resonators, we use two excitation schemes, namely optical drive and non-contact electrical drive, to actuate both bulk and flexural modes. Optical excitation is achieved with a 405nm RF-modulated diode laser whose frequency and amplitude are controlled by a NA. Electrical drive of the device motion, on the other hand, is enabled by the non-contact overhanging electrode. The electrode is made of copper with a thickness of 100µm. The applied voltage is tuned by the NA and sent to the non-contact overhanging electrode. The device resonant motion is subsequently read out via the optical interferometry with a 633nm laser (Fig. 1d). The laser interferometric signal is collected by a photodetector and measured by the NA. 'Knife-edge' effect measurement techniques are adopted to sensitively detect in-plane bulk modes of the BARs. Furthermore, the FEM analysis in COMSOL Multiphysics™ allows us to estimate resonance frequency and visualize mode shapes

for each device (Fig. 1a to 1c).

RESULTS AND DISCUSSIONS

Experimentally, we first actuate the out-of-plane flexural mode using both optical drive and non-contact electrical drive. With optical excitation, the blue laser is positioned at the center of the device to efficiently excite the out-of-plane motion. With electrical excitation, the overhanging electrode covering half of the device area is vertically ~200µm separated from the device surface. For the detection, the red-laser spot is parked on the device so only the out-of-plane motion can be detected. The experimental resonance curves measured by using the two techniques are displayed in Fig. 4. Both schemes resolve this mode at around f_1=595.35kHz. From the fitting (red dashed) curves, we also extract very similar Qs of ~1,400. Therefore, in characterizing the out-of-plane flexural mode, the non-contact electrical drive scheme works similarly as the optical drive scheme, in terms of Q.

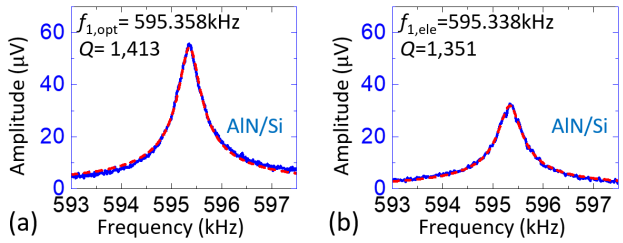

Figure 4: Response of the 1st flexural mode of the AlN/Si resonator using (a) optical and (b) non-contact electrical drive with applied v_{drv} of 200mV and 1.2V, respectively.

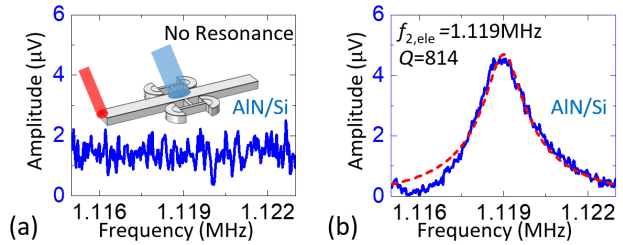

Figure 5: (a) Optical drive (blue laser) yields no signal of in-plane flexural mode. (b) Non-contact electrical drive yields clear resonance of in-plane flexural mode.

To investigate in-plane resonance modes of these devices, we reconfigure the detection scheme based on the 'knife-edge' optical readout techniques. In this scheme, the 633nm laser is gradually moved to the edge of the device until approximately ~30% of the spot area covers across the edge of the device. Such a configuration gives a high responsivity to convert signal from displacement domain to the optical domain, for in-plane lateral motion. Mode shapes from COMOSL simulation indicate that the AlN/Si device inherently has a laterally vibrating flexural mode at f_2=1.12MHz, as shown in Fig. 1b. However, this resonance is not visible when optical driving scheme is employed, whereas the non-contact electrical drive reveals this resonance at 1.119MHz with the fitting showing Q=814 (Fig. 5b). The actuation from non-contact electrical drive, thereby, provides AlN/Si device with sufficient energy to excite this in-plane flexural mode.

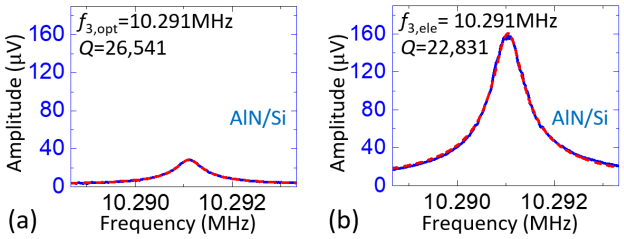

Figure 6: Resonance of the LE bulk mode of the AlN/Si resonator using (a) optical (blue laser) drive and (b) non-contact electrical drive.

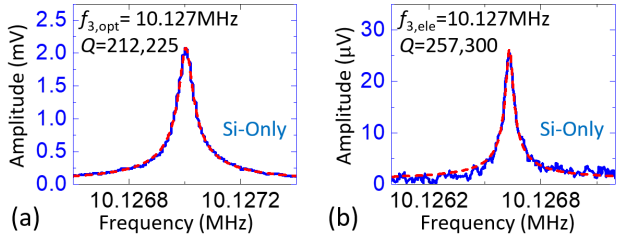

Figure 7: (a) Optically driven and (b) non-contact electrically driven response of the Si-only device. Non-contact electrical drive enables higher Q of the device indicating less energy loss than the optical drive.

We then focus on measuring the in-plane bulk mode of the AlN/Si resonator. The two peaks in Fig. 6 correspond to a same f_3=10.291MHz and a Q of~26,000, as observed by using both excitation schemes. For AlN/Si device, we find that all modes with optical drive present comparable Qs to that with electrical drive (Table 1), which may indicate negligible heating effect induced by laser. This could be attributed to the high thermal conductivity (321W/(m·K)) of AlN that expedites the heat conduction and results in a near uniform temperature distribution.

The dissipation in our device is related to various energy loss mechanisms [9] including thermoelastic damping Q^{-1}_{ted}, piezoelectric loss Q^{-1}_{pl}, dielectric loss Q^{-1}_{dl}, charge redistribution loss Q^{-1}_{cr}, anchor loss Q^{-1}_{al}, *etc.*,

$$\left(\frac{1}{Q}\right)_{tot} = \left(\frac{1}{Q}\right)_{ted} + \left(\frac{1}{Q}\right)_{pl} + \left(\frac{1}{Q}\right)_{dl} + \left(\frac{1}{Q}\right)_{cr} + \left(\frac{1}{Q}\right)_{al} + \cdots \quad (2)$$

In LE mode resonators, the main dissipation mechanism in AlN/Si devices is thermoelastic damping Q^{-1}_{ted} from the columnar boundary of AlN attained during the growth process [7]. To confirm the effect of the top piezoelectric AlN layer on the Q, we measure the same bulk mode of the Si-only device as a control experiment. Figure 7a presents the optically driven response with $f_{3,opt}$=10.127MHz and Q>200,000. The main raise in Q (8 times higher) when AlN layer is removed appears to be comparable with our expectation as the deposition of AlN layer greatly degrades the device Q. Furthermore, we excite the Si-only device using the non-contact electrical drive. Resonance frequency is very similar in value to that by optical drive. However, it manifests a Q that is 21% higher than the value measured with optical drive. A relatively smaller Q using blue-laser drive is probably related to laser heating effect caused by large optical absorption in the device Si layer. To validate our assumption, we theoretically calculate the optical power absorbed by the Si layer. The analysis of overall reflectance defined as a ratio of the total reflected

light over the incident light intensity [10] shows that the total reflected light takes up 47.8% of incident light. We then calculate the transmitted light and find that less than ~0.1% of incident light power is dissipated into the bottom electrode. Therefore, our 20μm Si device absorbs more than 52% of the photon energy from the blue laser. Moreover, a modest thermal conductivity (130W/(m·K)) of Si easily leads to temperature gradients in the device structure and thus introduces more intrinsic thermoelastic damping, which further degrades Q. The difference in Qs between two excitation schemes indicates that non-contact electrical drive scheme can be advantageous in reducing loss and attaining higher Q. Measured Qs of different modes are summarized in Table 1.

Table 1. Q factors of different modes measured with optical and electrical drive.

Modes / *Stack*	Out-of-Plane Flexural f_1 = 595.36kHz		In-Plane Flexural f_2 = 1.119MHz		Length Ext. Bulk Mode f_3 = 10.291MHz	
	$Q_{opt,drv}$	$Q_{ele,drv}$	$Q_{opt,drv}$	$Q_{ele,drv}$	$Q_{opt,drv}$	$Q_{ele,drv}$
AlN/Si	1,413	1,351	NA	814	26,541	22,831
Si-Only	NA	2,825	1,386	1,697	212,225	257,300

To gain further insight into the non-contact electrical excitation scheme, we measure the response of the devices with increasing drive amplitude. We gradually shift the drive voltage from 0V to 1.2V while recording the interrelated amplitude from the NA. Such voltage dependence of the amplitude for the bulk mode of AlN/Si and Si-only devices are presented in Fig. 8a and 8b, respectively. The devices display larger amplitudes with increasing RF voltage. As expected, a linear relationship between device motion and electrical drive is found (Fig. 8 insets) with the bulk modes still detectable at v_{drv}=0.2V.

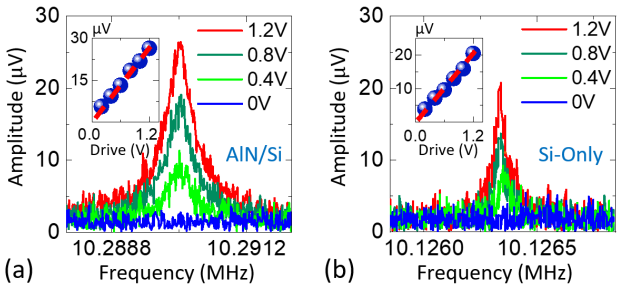

Figure 8: Measured responses of electrically driven (a) AlN/Si and (b) Si-only resonators with increasing RF driving voltage. Insets show resonance amplitude versus drive voltage. Measured data show a linear relationship between the measured amplitude and drive voltage.

CONCLUSION

In summary, we have demonstrated and analyzed a non-contact electrical drive for efficiently exciting AlN/Si heterostructure and Si-only MEMS resonators. Inverse piezoelectric effect in AlN and gradient forces emerging from electric field gradients are harnessed to drive resonance motions for bulk and flexural modes. The overhanging electrode allows for a convenient electrical excitation bypassing the otherwise required metal deposition and reduces the number of layers in the device heterostructure. We further compare the resonances of Si-only device using optical and electrical drive and attain a ~21% higher Q with electrical drive. The higher energy loss in photothermal actuation is attributed to heating effect as a result of considerable light absorption in the Si layer. Drive voltage dependence of device motion shows a linear relationship with detectable signal at 0.2V drive. The findings of using non-contact electrical drive may help enable low-loss, all-electrical transduction schemes and optimizing performance of MEMS resonators.

ACKNOWLEDGEMENTS

The effort at University of Florida (UF) is partly supported by NSF (Grant CCF-2103091) and by the Margaret A. Ross Scholarship (S M Enamul Hoque Yousuf) in ECE at UF.

REFERENCES

[1] R. Abdolvand, *et al.*, "Thin-film piezoelectric-on-silicon resonators for high-frequency reference oscillator applications", *IEEE Trans. Ultrason. Ferroelectr. Freq. Control*, vol. 55, pp. 2596-2606, 2008.

[2] J. L. Fu, *et al.*, "Dual-mode AlN-on-silicon micromechanical resonators for temperature sensing", *IEEE Trans. Electron Devices*, vol. 61, pp. 591–597, 2014.

[3] S. Strite, *et al.*, "GaN, AlN, and InN: a review", *J. Vac. Sci. Technol. B,* vol. 10, pp. 1237–1266, 1992.

[4] X.-H. Xu, *et al.*, "Morphological properties of AlN piezoelectric thin films deposited by DC reactive magnetron sputtering", *Thin Solid Films*, vol. 388, pp. 62–67, 2001.

[5] G. K. Ho, *et al.*, "Piezoelectric-on-silicon lateral bulk acoustic wave micromechanical resonators", *J. Microelectromech. Syst.*, vol. 17, pp. 512–520, 2008.

[6] A. Qamar, *et al.*, "Solidly mounted anti-symmetric Lamb-wave delay lines as an alternate to saw devices", *IEEE Electron Device Lett.*, vol. 39, pp. 1916–1919, 2018.

[7] A. Qamar, *et al.*, "Study of energy loss mechanisms in AlN-based piezoelectric length extensional-mode resonators", *J. Microelectromech. Syst.*, vol. 28, pp. 619–627, 2019.

[8] Q. P. Unterreithmeier, *et al.*, "Universal transduction scheme for nanomechanical systems based on dielectric forces", *Nature*, vol. 458, pp. 1001–1004, 2009.

[9] X. L. Feng, *et al.*, "Dissipation in single-crystal 3C-SiC ultra-high frequency nanomechanical resonators", in *Tech. Digest of Hilton Head'06*, June 4-8, 2006, pp. 86–89.

[10] P. Blake, *et al.*, "Making graphene visible", *Appl. Phys. Lett.*, vol. 91, art. no. 063124, 2007.

CONTACT

†*Equally Contributed Authors*
*†S M Enamul Hoque Yousuf: syousuf@ufl.edu
*†Yuncong Liu: yuncong.liu@ufl.edu
* Mina Rais-Zadeh: mina.rais-zadeh@jpl.nasa.gov
* Philip Feng: philip.feng@ufl.edu